A FAST ALGORITHM FOR SPHERICAL BASIS APPROXIMATION

J. KEINER, J. PRESTIN

Abstract. Radial basis functions appear in a wide field of applications in numerical mathematics and computer science. We present a fast algorithm for scattered data interpolation and approximation on the sphere with spherical radial basis functions of different spatial density. We discuss three settings, each leading to a special structure of the interpolation matrix allowing for an efficient implementation using discrete Fourier transforms. A numerical example is given to show the advantages of spherical radial basis functions with different spatial densities.

2000 *A*MS Subject Classification: 65T50, 65F30, 33C55, 15A23, 41A30.
Key words and phrases: Radial basis functions, circulant matrices, FFT.

1. Introduction

Radial basis functions have spread into a wide field of topics in numerical mathematics and computer science. Applications can be found in approximation of high dimensional and/or scattered data and the modelling of partial differential equations, as well as in neuroinformatics where so-called *radial basis function networks* are prominent. Not only for the mentioned applications, these functions are of special interest, since they show several features which make them well suited for a wide range of problems and, at the same time, computationally attractive (cf. e.g. [3] and the references therein).

The characteristic property of radial basis functions is that their value only depends on the "distance" of the argument to a fixed element of the function's domain. To be more exact, a radial basis function f is given by

$$f : V^2 \to \mathbb{C},\ f(x,y) := \tilde{f}(\|x-y\|),\ \tilde{f} : \mathbb{R}^+ \to \mathbb{C},\ x,y \in V,$$

where $(V, \|\cdot\|)$ is a metric space. The definition shows clearly that calculations are simplified, since radial basis functions behave like univariate functions, although their domain, in general, is multi-dimensional. Especially for higher dimensions, this fact contributes at a considerable amount to the effectiveness of algorithms which utilise these functions.

Moreover, many radial basis functions have physical interpretations making them a reasonable choice for the modelling of many physically motivated problems. The Poisson kernel for example, a function we will study in this paper, can be viewed as a solution of a potential problem, which makes it particularly useful for a range of problems on spherical geometries.

From another point of view, the use of radial basis functions for approximation problems becomes more clear: They can be used to interpolate functions from a given set of scattered data points without requiring a certain structure with respect to their distribution in the domain. We can think of a set of these functions, where each of them is associated with exactly one of the data points and models the influence of it on a probabilistic model of the function to be approximated. A model function can be derived as a linear combination of these functions. For reasonable

choices, they are often unimodal and show exactly one global maximum at a certain point, often referred to as their *centre*. Therefore, each function's influence on the model function decreases as one moves away from it's centre, which, besides from being somewhat reasonable in many cases, leads to a stability property of the interpolating function. Deviations of a single data point only become visible in it's neighbourhood.

In this paper, we deal with a setting where we like to describe real-valued functions, defined on a two-dimensional sphere embedded in the Euclidean space $\mathbb{R}^3$. Section 2 gives a quick introduction to notational conventions used and special properties of spherical geometry.

In Section 3 we review *Legendre polynomials*, *associated Legendre functions* and *spherical harmonics*. These functions and the underlying concepts form the classical basement for spherical approximation.

The following Section 4 introduces the concept of *spherical basis functions* and in particular *positive definite functions*. They represent an entirely different approach compared to spherical harmonics, which is well suited in cases where spherical harmonics tend to exhibit unwanted ripple structures in the approximating function. This can be often observed when somewhat *smooth* data with only a few protruding peaks serves as input. As we will see, spherical basis functions can master this situation quite well. For error estimates and further applications we refer to [6, 7]. Moreover, we exploit the idea of using different kinds of functions to represent regions of different smoothness in the data. The geometry of the sphere itself renders this uniform approach often useless by causing the same type of problems. In conclusion, we show the linear independence of Poisson kernels of pairwise different parametrisation. For a more general approach to multiscale kernels see [11].

Section 5 formulates some algorithmic aspects which arise in spherical approximation with radial basis functions. We refer the reader also to [8]. Some symmetry properties are derived and it is shown how they can be exploited to reduce computational costs. But as a warning, the amount of reduction that can be achieved, strongly depends on the concrete distribution of the given data.

Finally, Section 6 shows applications of the concepts introduced in the previous sections to real-life data from texture analysis in crystallography (see [2]). We demonstrate that for these data sets, a multiscale approach incorporating Poisson kernels or other radial basis functions of different "shape" is obligate for a good approximation result.

2. Basics

Every point $\mathbf{x} \in \mathbb{R}^3 \backslash \{\mathbf{0}\}$ given in Cartesian coordinates by the vector $(x_1, x_2, x_3)^{\mathrm{T}}$ can be described in spherical coordinates by a vector $(r, \vartheta, \varphi)^{\mathrm{T}}$ with $r \in \mathbb{R}^+$, $\vartheta \in [0, \pi]$ and $\varphi \in [0, 2\pi)$ (see Figure 2.1). We have

$$\begin{aligned} (x_1, x_2, x_3)^{\mathrm{T}} &= (r \sin\vartheta \cos\varphi, r \sin\vartheta \sin\varphi, r \cos\vartheta)^{\mathrm{T}}, \\ r &= \sqrt{x_1^2 + x_2^2 + x_3^2} = \|\mathbf{x}\|_2 . \end{aligned}$$

We denote by $\mathbb{S}^2$ the unit sphere embedded into $\mathbb{R}^3$, i.e.

$$\mathbb{S}^2 := \left\{ \mathbf{x} \in \mathbb{R}^3 \mid \|\mathbf{x}\|_2 = 1 \right\}$$

and identify $\xi \in \mathbb{S}^2$ with the vector $(\vartheta, \varphi)^{\mathrm{T}}$. Let $\xi = (\vartheta, \varphi)^{\mathrm{T}}$, $\eta = (\vartheta', \varphi')^{\mathrm{T}} \in \mathbb{S}^2$ and α be the angle spanned by the origin, ξ and η. Then the standard inner product $\xi \cdot \eta = \cos\alpha$ is given by

$$\cos\alpha = \cos\vartheta \cos\vartheta' + \sin\vartheta \sin\vartheta' \cos(\varphi - \varphi') .$$

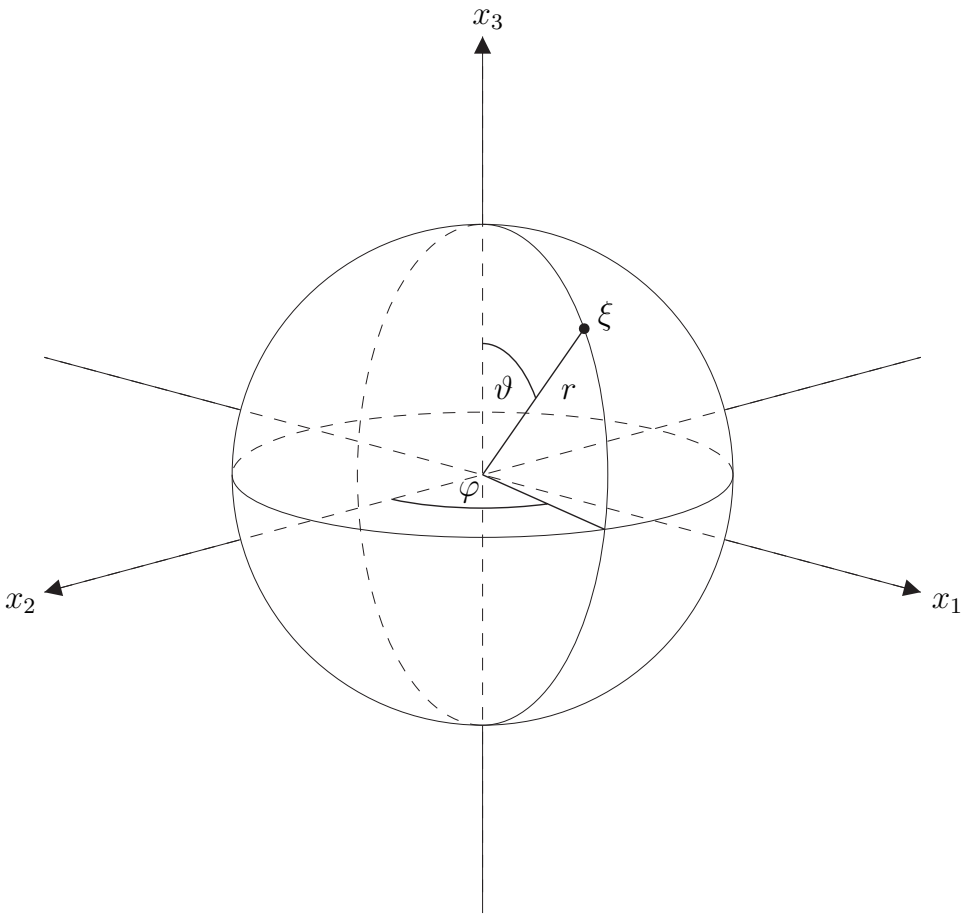

FIGURE 2.1. The spherical coordinate system in $\mathbb{R}^3$. Every point ξ on a sphere with radius r around the origin can be described by angles ϑ, φ and the radius r. For $\vartheta = 0$ or $\vartheta = \pi$ the point ξ coincides with the North or the South pole, respectively.

The space of *homogeneous polynomials* of degree $k \in \mathbb{N}_0$ in $\mathbb{R}^3$ is denoted by $\mathrm{Hom}_k\left(\mathbb{R}^3\right)$, comprising all polynomials $Q_k \in \Pi_k\left(\mathbb{R}\right)$ fulfilling $Q_k\left(\alpha\,\mathbf{x}\right) = \alpha^k Q_k\left(\mathbf{x}\right)$ for arbitrary $\alpha \in \mathbb{R}$ and $\mathbf{x} \in \mathbb{R}^3$. The proper subspace of *harmonic homogeneous polynomials* of degree k is defined by

$$\mathrm{Harm}_k\left(\mathbb{R}^3\right) := \left\{ Q_k \in \mathrm{Hom}_k\left(\mathbb{R}^3\right) \mid \Delta_{\mathbf{x}} Q = 0 \right\},$$

where $\Delta_{\mathbf{x}}$ is the Laplacian

$$\Delta_{\mathbf{x}} := \frac{\partial^2}{\partial x_1^2} + \frac{\partial^2}{\partial x_2^2} + \frac{\partial^2}{\partial x_3^2}.$$

Furthermore, we have

$$\dim\left(\mathrm{Hom}_k\left(\mathbb{R}^3\right)\right) = \frac{(k+1)(k+2)}{2},\ \dim\left(\mathrm{Harm}_k\left(\mathbb{R}^3\right)\right) = 2k+1.$$

To keep it short, we let $\mathcal{H}_k := \mathrm{Harm}_n\left(\mathbb{R}^3\right)\big|\,\mathbb{S}^2$. For further details see [5] or [10].

The description of the spherical approximation problem starts with a given finite dimensional space $\mathcal{V}$ with dimension $K \in \mathbb{N}$ of square integrable functions $\psi : \mathbb{S}^2 \to$

$\mathbb{R}$, hence

$$\int_{\mathbb{S}^2} |\psi(\xi)|^2 \,\mathrm{d}\xi := \int_0^{2\pi} \int_0^{\pi} |\psi(\vartheta,\varphi)|^2 \sin\vartheta \,\mathrm{d}\vartheta \,\mathrm{d}\varphi < \infty.$$

With respect to a basis $\{\psi_k\}_{k=1}^K$ of $\mathcal{V}$, every function $f \in \mathcal{V}$ has a unique representation

$$f = \sum_{k=1}^{K} a_k(f)\,\psi_k \quad (a_k \in \mathbb{R}).$$

In our setting, we are given data points $(\xi_l, f_l)_{l=1}^L$, $L \in \mathbb{N}$, with $\xi_l \in \mathbb{S}^2$ and $f_l \in \mathbb{R}$. We let

$$\mathbf{f} := (f_1,\ldots,f_L)^{\mathrm{T}} \in \mathbb{R}^L,\ \mathbf{a} := (a_1,\ldots,a_K)^{\mathrm{T}} \in \mathbb{R}^K$$

and

$$\mathbf{\Psi} := \begin{pmatrix} \psi_1(\xi_1) & \ldots & \psi_K(\xi_1) \\ \vdots & \ddots & \vdots \\ \psi_1(\xi_L) & \ldots & \psi_K(\xi_L) \end{pmatrix} \in \mathbb{R}^{L\times K}. \tag{2.1}$$

The approximation problem on the sphere reads as follows:

$$\text{Find } \tilde{\mathbf{a}} \in \mathbb{R}^K \text{ satisfying } \tilde{\mathbf{a}} \in \arg\min_{\mathbf{a}\in\mathbb{R}^K} \|\mathbf{f} - \mathbf{\Psi}\,\mathbf{a}\|_2 .$$

Depending on which case holds, $K \le L$ or $K > L$, the problem can be viewed as a *least-squares-problem* or as a so-called *special optimisation problem*. For the topics treated in this text, $K = L$ holds and $\mathbf{\Psi}$ will be assumed to be non-singular, so that the solution can be explicitly written as

$$\tilde{\mathbf{a}} = \mathbf{\Psi}^{-1}\mathbf{f}.$$

For further information we refer the interested reader to [1].

3. Legendre Functions and Spherical Harmonics

We briefly mention some facts on *Legendre polynomials* and the closely related *associated Legendre functions*. Based on this foundation, we describe the function space of spherical harmonics and how it is related to spherical approximation.

The Legendre polynomials $P_k : [-1,1] \to \mathbb{R}$, $k \in \mathbb{N}_0$, as classical orthogonal polynomials are given by their corresponding *Rodrigues formula*

$$P_k(t) := \frac{1}{2^k k!}\frac{\mathrm{d}^k}{\mathrm{d}t^k}\left(t^2-1\right)^k.$$

The *Formula of Laplace-Heine* ([**]szegoe:1939p. 194) provides a classical asymptotic approximation formula for Legendre polynomials: It says that for $k \in \mathbb{N}$ and $\vartheta \in [\epsilon, \pi-\epsilon]$ with $\epsilon > 0$ we have

$$P_k(\cos\vartheta) = \sqrt{\frac{2}{\pi k \sin\vartheta}}\cos\left(\left(k+\frac{1}{2}\right)\vartheta - \frac{\pi}{4}\right) + \mathcal{O}\left(k^{-3/2}\right). \tag{3.1}$$

Concerning the generating series of the Legendre polynomials

$$\phi(h,t) := \sum_{k=0}^{\infty} P_k(t)\,h^k \tag{3.2}$$

for arbitrary but fixed $t \in [-1,1]$, which is absolutely and uniformly convergent for $h \in (-1,1)$, we have

$$\sum_{k=0}^{\infty} P_k(t)\,h^k = \frac{1}{\sqrt{1-2ht+h^2}}. \tag{3.3}$$

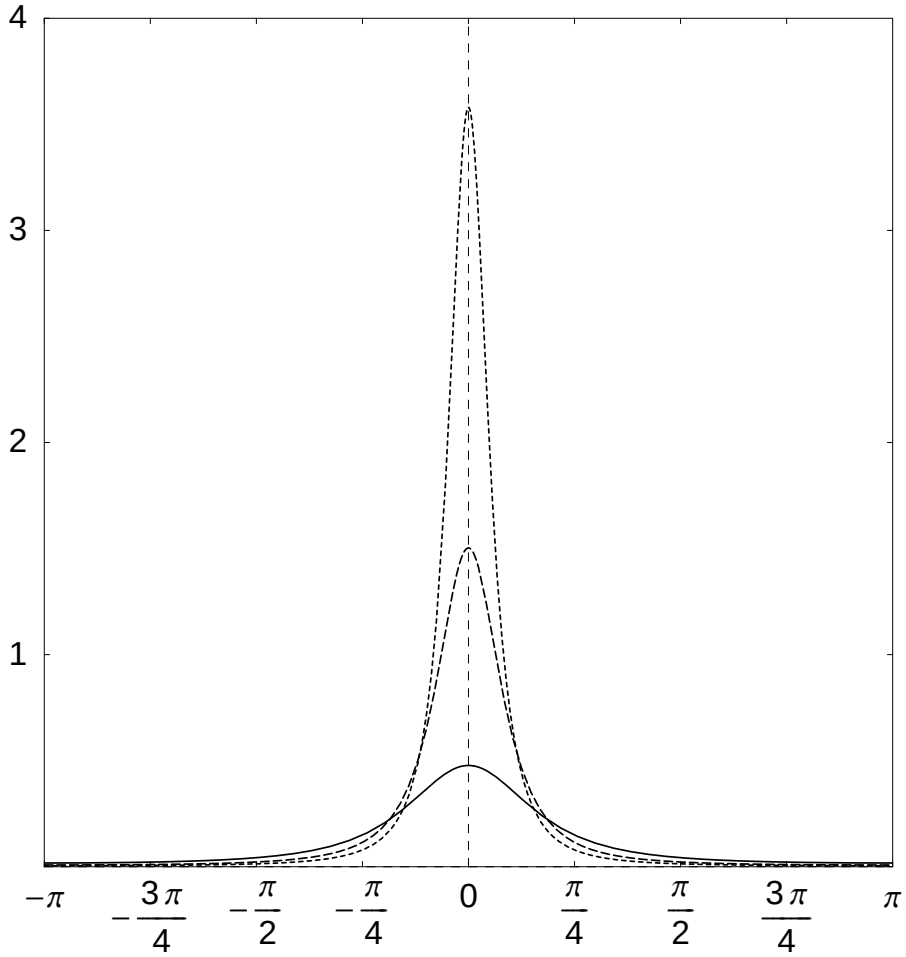

FIGURE 3.1. The Poisson kernel $Q_h(\cos\vartheta)$ for $h = 0.5, 0.7, 0.8$. The energy concentrates more and more around $\vartheta = 0$ as h increases.

This representation follows from the ordinary differential equation

$$\left(1 + h^2 - 2ht\right)\left(\frac{\partial}{\partial h}\phi\right)(h,t) = (t-h)\,\phi(h,t) \tag{3.4}$$

obtained by differentiation with respect to h and comparing coefficients in line with (3.2). Using the initial condition $\phi(0,t) = 1$ yields the unique solution (3.3). From this result, the identity

$$\sum_{k=0}^{\infty} (2k+1)\,P_k(t)\,h^k = \frac{1-h^2}{(1-2ht+h^2)^{3/2}}$$

follows easily.

When h is restricted to $(0,1)$, the function $Q_h : [-1,1] \to \mathbb{R}$ with

$$Q_h(t) := \frac{1-h^2}{(1-2ht+h^2)^{3/2}} \tag{3.5}$$

is called *Poisson kernel*. We refer to Figure 3.1 and notice that the parameter h allows for controlling the concentration of the function's energy around $t = 1$.

The Legendre polynomials can be viewed as a special case of a more general set of orthogonal functions. Let $k, n \in \mathbb{N}_0$ with $n \le k$. The functions $P_k^n : [-1,1] \to \mathbb{R}$, given by

$$P_k^n(t) := \left(\frac{(k-n)!}{(k+n)!}\right)^{1/2} \left(1-t^2\right)^{n/2} \frac{\mathrm{d}^n}{\mathrm{d}t^n} P_k(t),$$

are called associated Legendre functions.

Notice that the associated Legendre function P_k^0 coincides with the Legendre polynomial P_k. The associated Legendre functions fulfil the orthogonality condition

$$\int_{-1}^{1} P_k^n(t) P_l^n(t) \, \mathrm{d}t = \frac{2}{2k+1} \delta_{k,l} \quad (n \le \min\{k,l\}).$$

We now introduce the function space of *spherical harmonics*, a key to the treatment of spherical approximation problems. From Laplace's differential equation $\Delta f = \mathbf{0}$ in $\mathbb{R}^3$ one obtains in spherical coordinates

$$\Delta f = \frac{\partial^2 f}{\partial r^2} + \frac{2}{r}\frac{\partial f}{\partial r} + \frac{1}{r^2 \sin\vartheta}\frac{\partial}{\partial \vartheta}\left(\sin\vartheta \cdot \frac{\partial f}{\partial \vartheta}\right) + \frac{1}{r^2 \sin\vartheta}\frac{\partial^2 f}{\partial \varphi^2} = 0. \tag{3.6}$$

Using an ansatz based on separation of variables and taking into account that $r = 1$ when restricting (3.6) to $\mathbb{S}^2$, one obtains the solutions

$$\begin{aligned} &Y_k^n : \mathbb{S}^2 \to \mathbb{C} \quad (k \in \mathbb{N}_0;\ n = -k, -k+1, \ldots, k), \\ &Y_k^n(\vartheta,\varphi) := \sqrt{\frac{2k+1}{4\pi}} P_k^{|n|}(\cos\vartheta)\, \mathrm{e}^{\mathrm{i}n\varphi}. \end{aligned} \tag{3.7}$$

An important result is that these functions Y_k^n are contained in $\mathcal{H}_k$. Owing to the separability one proves easily that they also fulfil the orthogonality condition

$$\langle Y_k^n, Y_l^m \rangle_{\mathbb{S}^2} = \delta_{k,l}\, \delta_{n,m}$$

with respect to the $\mathrm{L}^2\left(\mathbb{S}^2\right)$-inner product

$$\langle Y_k^n, Y_l^m \rangle_{\mathbb{S}^2} := \int_0^{2\pi} \int_0^{\pi} Y_k^n(\vartheta,\varphi)\, \overline{Y_l^m(\vartheta,\varphi)} \sin\vartheta \, \mathrm{d}\vartheta \, \mathrm{d}\varphi.$$

Since $\dim \mathcal{H}_k = 2k+1$, the set $\{Y_k^n \mid n = -k, -k+1, \ldots, k\}$ forms an orthonormal basis of $\mathcal{H}_k$ for every $k \in \mathbb{N}_0$. Moreover, the spaces $\mathcal{H}_k$ are orthogonal to each other and the set

$$\{Y_k^n \mid k = 0, 1, \ldots, K;\ n = -k, -k+1, \ldots, k\} \quad (K \in \mathbb{N}_0)$$

provides an orthonormal basis for the direct sum of spaces $\bigoplus_{k=0}^{K} \mathcal{H}_k$ called the space of *spherical harmonics* of degree K.

At first glance, the restriction to homogeneous and harmonic polynomials might exclude various functions from $\Pi_K\left(\mathbb{S}^2\right)$. But as a matter of fact, the spaces are identical (see [5, p. 29]), i.e.

$$\Pi_K\left(\mathbb{S}^2\right) = \bigoplus_{k=0}^{K} \mathcal{H}_k.$$

Finally, we mention the well known *Addition Theorem* that relates any set of functions $\{H_k^n\}_{n=-k}^{k}$ forming an orthonormal basis of the space $\mathcal{H}_k$ to the Legendre polynomials P_k. It particularly holds for the basis given in (3.7).

Proposition 3.1 (Addition Theorem)**.** *For every $L^2\left(\mathbb{S}^2\right)$-orthonormal basis $\{H_k^n\}_{n=-k}^{k}$ of $\mathcal{H}_k$, we have*

$$\sum_{n=-k}^{k} H_k^n(\xi)\, \overline{H_k^n(\eta)} = \frac{2k+1}{4\pi} P_k(\xi \cdot \eta).$$

For a proof see [10] or [5, p. 37].

4. Spherical Basis Functions

In this section we introduce an alternative suitable class of functions for approximation on the sphere - namely *spherical basis functions*. Instead of providing a basis for a certain function space on the sphere directly, the space of spherical basis functions covers a wide range of functions, where each of them generates a basis for an approximation space that is suited for a given set of data points. This allows to adjust the used space to the properties of the given data in order to achieve optimal results, making spherical basis functions more flexible and useful especially for scattered data. Strongly correlated with spherical basis functions is the class of *positive definite functions*.

Definition 4.1. A continuous function $G : [-1, 1] \to \mathbb{R}$ is called *positive definite*, if and only if for every set of points $\{\xi_l\}_{l=1}^{L}$ on $\mathbb{S}^2$, $L \in \mathbb{N}$, the corresponding *Gramian matrix* $\mathbf{A} := (a_{i,j})_{i,j=1}^{L}$ with $a_{i,j} := G(\xi_i \cdot \xi_j)$ is positive semi-definite. If $\mathbf{A}$ is even positive definite, G is called a *strictly positive definite function*.

In general, it is hard to prove directly that a function is positive definite according to Definition 4.1. A fundamental characterisation is given in the following theorem due to Schoenberg (see [12]).

Proposition 4.2. *Let $G : [-1, 1] \to \mathbb{R}$ be a function of the form $G = \sum_{k=0}^{\infty} a_k P_k$, with $\sum_{k=0}^{\infty} |a_k| < \infty$. Then the following statements are equivalent:*

1. *The function G is positive definite on $\mathbb{S}^2$.*
2. *The coefficients a_k fulfill $a_k \geq 0$ for all $k \in \mathbb{N}_0$.*

For strictly positive definite functions a similar necessary and sufficient condition was proved recently by Chen, Menegatto and Sun in [4]: A function G is strictly positive definite if and only if all coefficients a_k are greater than or equal to zero and infinitely many coefficients a_k with odd k and infinitely many coefficients a_k with even k are greater than zero. Now, for our purpose spherical basis functions are defined as follows:

Definition 4.3. Every function $G : [-1, 1] \to \mathbb{R}$ with

$$G(t) = \sum_{k=0}^{\infty} a_k P_k(t),$$

satisfying $a_k > 0$ for all $k \in \mathbb{N}_0$ and $\sum_{k=0}^{\infty} a_k < \infty$ is called a *spherical basis function*.

The Poisson kernel Q_h defined in (3.5), for example, is a spherical basis function. This follows immediately taking into account that $(2k+1)\,h^k > 0$ for all $k \in \mathbb{N}_0$ and $\sum_{k=0}^{\infty} (2k+1)\,h^k < \infty$ for $h \in (0, 1)$.

Using spherical basis functions, we define the approximation space and a basis in order to use the scheme from Section 2. Given data points $(\xi_l, f_l)_{l=1}^{L}$, $L \in \mathbb{N}$ and having chosen a spherical basis function G, we obtain the functions $G_l : \mathbb{S}^2 \mapsto \mathbb{R}$ by

$$G_l(\xi) := G(\xi_l \cdot \xi).$$

The values of the generated functions G_l solely depend on the geodesic distance of the argument ξ to the fixed point ξ_l. For many reasonable choices, the function value reaches a maximum at $\xi = \xi_l$ and decreases towards a minimum for $\xi = -\xi_l$. Figure 4.1 shows the Poisson-kernel $Q_h\left((0,0)^{\mathrm{T}} \cdot \xi\right)$ centred at the North pole for different values of h.

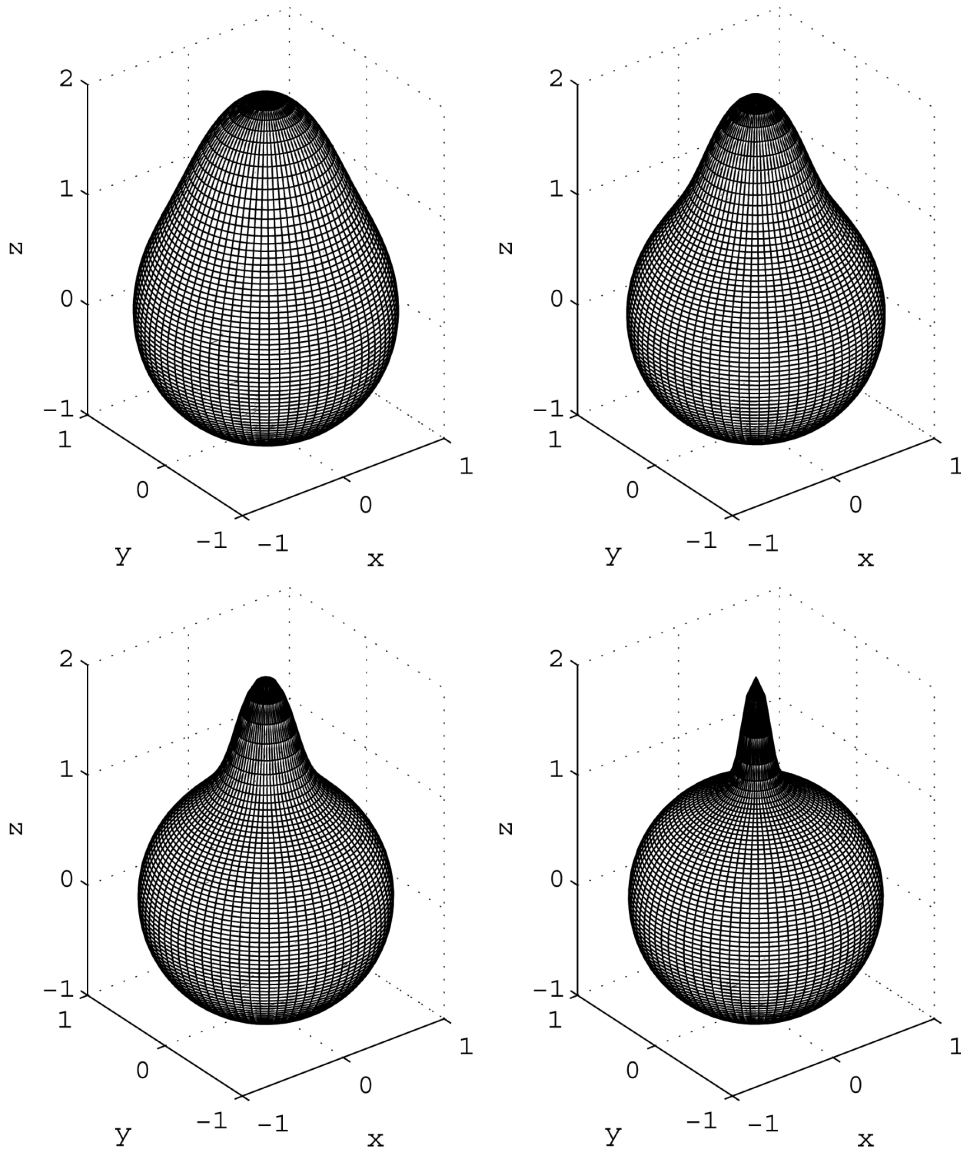

FIGURE 4.1. The Poisson-kernel $Q_h\left((0,0)^{\mathrm{T}} \cdot \xi\right)$ centred at the North pole as a function of ξ and evaluated on the sphere $\mathbb{S}^2$ for different values of h. Starting with $h = 0.6$ in the upper left picture, the value increases in steps of 0.1 to $h = 0.9$ in the lower right picture.

Now, the matrix $\mathbf{\Psi}$ introduced in (2.1) is in this setting identical to the Gramian matrix from Definition 4.1, which is known to be positive definite, hence regular. Notice that this property immediately implies the linear independence of the functions G_l.

From a more practical point of view, a drawback of the described method becomes clear. Independent of the distribution of the points ξ_l on the sphere, all data samples are represented by rotated versions of the same function with same spatial density generated from a single spherical basis function G. As it is often the case in practical situations, the data do not need to be distributed uniformly. Data points

can be clustered in certain regions, while in others their density might be low. This can cause problems in the quality of the computed approximation result and leads to numerical instability. Another aspect is that these functions can also be used for multiscale representations, where, depending on the required accuracy, a subset of the basis functions is used to represent either a fine or a coarse approximation. Here, the need for functions of different spatial density is also essential.

As well as the use of this more flexible approach seems to be working (see for example [9]), theoretic results ensuring the solvability of the problem for sets of possibly different basis functions are not easy to obtain. In the next section, we will show the linear independence of Poisson kernels for pairwise different parameter h. But it will remain open whether the matrix $\mathbf{\Psi}$ still remains non-singular.

4.1. **Extension to the Multiscale Case.** In order to investigate the linear independence of Poisson kernels at different scales, i.e. for different values of h, we first need some basic results.

Lemma 4.4. *Let $\vartheta \in [0, \pi]$ be fixed. There exists a constant $c(\vartheta) > 0$ such that for arbitrary $k \in \mathbb{N}_0$ there exists an index $k^* \in \mathbb{N}_0$ with $k^* \geq k$ and*

$$\sqrt{\frac{2k^*+1}{4\pi}} \left| P_{k^*}(\cos\vartheta) \right| > c(\vartheta). \tag{4.1}$$

Proof. The case $k = 0$ is trivial since $P_0 = 1$. So let $k > 0$ and assume at first $\vartheta = 0$ or $\vartheta = \pi$. By observing $|P_k(\cos\vartheta)| = |P_k(\pm 1)| = 1$, we obtain the estimate

$$\sqrt{\frac{2k+1}{4\pi}} \left| P_k(\cos\vartheta) \right| = \sqrt{\frac{2k+1}{4\pi}} \geq \frac{1}{2\sqrt{\pi}} > 0.$$

By choosing $k^* = k$ and $c(\vartheta) \in \left(0, \frac{1}{2\sqrt{\pi}}\right)$ arbitrary, assertion (4.1) is fulfilled. Now fix $\vartheta \in (0, \pi)$. Employing the approximation formula from (3.1) we conclude

$$\sqrt{\frac{2k+1}{4\pi}} \left| P_k(\cos\vartheta) \right| = \frac{1}{\pi\sqrt{\sin\vartheta}} \left| \cos\left(\left(k + \frac{1}{2}\right)\vartheta - \frac{\pi}{4} \right) \right| + \mathcal{O}\left(k^{-1}\right).$$

The asymptotic part $\mathcal{O}\left(k^{-1}\right)$ vanishes for $k \to \infty$. The constant $\frac{1}{\pi\sqrt{\sin\vartheta}}$ is strictly positive. So let us assume

$$\cos\left(\left(k + \frac{1}{2}\right)\vartheta - \frac{\pi}{4} \right) \xrightarrow{k\to\infty} 0.$$

We now immediately get a contradiction, since this would require ϑ to be of the form $\vartheta = j\pi$ for certain $j \in \mathbb{Z} \setminus \{0\}$ and would therefore violate the assumption $0 < \vartheta < \pi$. □

Corollary 4.5. *Let $\xi = (\vartheta, \varphi) \in \mathbb{S}^2$ be fixed. There exists a constant $c(\vartheta) > 0$ such that for arbitrary $k \in \mathbb{N}_0$ there exists an index $k^* \in \mathbb{N}_0$ with $k^* \geq k$ and*

$$\left| Y_{k^*}^0(\xi) \right| > c(\vartheta).$$

Proof. We utilise the definition of the functions Y_k^n in (3.7) with

$$Y_k^n(\vartheta, \varphi) = \sqrt{\frac{2k+1}{4\pi}} P_k^{|n|}(\cos\vartheta)\, e^{\mathrm{i}n\varphi},$$

and close with the remark that for $n = 0$, the proof reduces to an application of Lemma 4.4. □

Corollary 4.5 now allows for an investigation of the linear independence of Poisson kernels Q_h for pairwise different parameters h.

Theorem 4.6. *Let $L \in \mathbb{N}$, $0 < h_1 < h_2 < \cdots < h_L < 1$ and*

$$\xi_l := (\vartheta_l, \varphi_l) \in \mathbb{S}^2 \quad (l = 1, \ldots, L)$$

be L pairwise different points on the sphere. Then the functions $G_l : \mathbb{S}^2 \to \mathbb{R}$ with

$$G_l(\xi) := Q_{h_l}(\xi_l \cdot \xi) = \sum_{k=0}^{\infty} (2k+1) P_k(\xi_l \cdot \xi) h_l^k$$

are linearly independent.

Proof. We assume

$$\sum_{l=1}^{L} \lambda_l G_l(\xi_l \cdot \xi) = 0 \quad \left(\xi \in \mathbb{S}^2\right)$$

for certain coefficients $\lambda_i \in \mathbb{R}$ and prove that $\lambda_l = 0$ holds for $l = 1, \ldots, L$. Applying the definition of the Poisson kernel from (3.5) and using the Addition Theorem from Proposition 3.1, we obtain

$$\begin{aligned} 0 \;=\; \sum_{l=1}^{L} \lambda_l G_l(\xi_l \cdot \xi) &= \sum_{l=1}^{L} \lambda_l \sum_{k=0}^{\infty} (2k+1) P_k(\xi_l \cdot \xi) h_l^k \\ &= \sum_{l=1}^{L} \lambda_l \sum_{k=0}^{\infty} 4\pi\, h_l^k \sum_{n=-k}^{k} Y_k^n(\xi_l) \overline{Y_k^n(\xi)} \\ &= \sum_{k=0}^{\infty} \sum_{n=-k}^{k} \left(\sum_{l=1}^{L} \lambda_l\, 4\pi\, h_l^k\, Y_k^n(\xi_l) \right) \overline{Y_k^n(\xi)}. \end{aligned}$$

In view of the fact that the set $\left\{\overline{Y_k^n}\right\}_{k \in \mathbb{N}_0, n=-k,\ldots,k}$ forms a basis of $\mathrm{L}^2\left(\mathbb{S}^2\right)$, the following infinite set of equations

$$\sum_{l=1}^{L} \lambda_l\, h_l^k\, Y_k^n(\xi_l) = 0 \quad (k \in \mathbb{N}_0,\ n = -k, \ldots, k) \tag{4.2}$$

must be fulfilled. So assume now that there exists at least one index l such that $\lambda_l \neq 0$ and define

$$l_{\max} := \max_{l=1,\ldots,L} \{ l \mid \lambda_l \neq 0 \}.$$

Owing to the estimates

$$\left| \frac{(L-1)\lambda_l}{c\,\lambda_{l_{\max}}} \right| = \mathcal{O}(1), \quad \left(\frac{h_l}{h_{l_{\max}}} \right)^k = \mathcal{O}\left(e^{-k}\right), \quad \left|Y_k^0(\xi_l)\right| = \mathcal{O}\left(\sqrt{k}\right)$$

for $l = 1, \ldots, L$, where c is an arbitrary positive constant, we get

$$\lim_{k\to\infty} \frac{\left|\lambda_l\, h_l^k\, Y_k^0(\xi_l)\right|}{\left|\frac{c}{L-1}\lambda_{l_{\max}}\, h_{l_{\max}}^k\right|} = \lim_{k\to\infty} \left| \frac{(L-1)\lambda_l}{c\,\lambda_{l_{\max}}} \right| \left(\frac{h_l}{h_{l_{\max}}} \right)^k \left|Y_k^0(\xi_l)\right| = 0.$$

Now, using Corollary 4.5, let $k^* \in \mathbb{N}_0$ be large enough such that

$$\left|Y_{k^*}^0(\xi_{l_{\max}})\right| > c(\vartheta_{l_{\max}}) > 0$$

and

$$\left|\lambda_l\, h_l^{k^*}\, Y_{k^*}^0(\xi_l)\right| < \left| \frac{c(\vartheta_{l_{\max}})}{L-1} \lambda_{l_{\max}}\, h_{l_{\max}}^{k^*} \right| \quad (l = 1, \ldots, L; l \neq l_{\max})$$

are simultaneously satisfied. We finally obtain

$$\begin{aligned}
\left|\sum_{l=1}^{L} \lambda_l \; h_l^{k^*} \; Y_{k^*}^0 \left(\xi_i\right)\right| \geq & \left|\lambda_{l_{\max}} \; h_{l_{\max}}^{k^*} \; Y_{k^*}^0 \left(\xi_{l_{\max}}\right)\right| - \sum_{\substack{l=1,\\ l\neq l_{\max}}}^{L} \left|\lambda_l \; h_l^{k^*} \; Y_{k^*}^0 \left(\xi_l\right)\right| \\
\geq & \left|\lambda_{l_{\max}} \; h_{l_{\max}}^{k^*} \; Y_{k^*}^0 \left(\xi_{l_{\max}}\right)\right| - \sum_{\substack{l=1,\\ l\neq l_{\max}}}^{L} \left|\frac{c\left(\vartheta_{l_{\max}}\right)}{L-1} \lambda_{l_{\max}} \; h_{l_{\max}}^{k^*}\right| \\
= & \left|\lambda_{l_{\max}} \; h_{l_{\max}}^{k^*} \; Y_{k^*}^0 \left(\xi_{l_{\max}}\right)\right| - \left|c\left(\vartheta_{l_{\max}}\right) \; \lambda_{l_{\max}} \; h_{l_{\max}}^{k^*}\right| \\
= & \left(\left|Y_{k^*}^0 \left(\xi_{l_{\max}}\right)\right| - c\left(\vartheta_{l_{\max}}\right)\right) \left|\lambda_{l_{\max}} \; h_{l_{\max}}^{k^*}\right| \\
> & \; 0,
\end{aligned}$$

which contradicts (4.2). □

5. Algorithmic Aspects

This section concentrates on facets in the numerical treatment of the spherical approximation problem with radial basis functions. We mention properties of the interpolation matrix $\mathbf{\Psi}$, explain under which conditions with respect to the data points they are present and briefly discuss how they can be exploited to reduce computational costs. We finally give an algorithm for a certain class of grids that achieves better asymptotic complexity than a naive approach.

When we talk about a spherical grid, we refer to a set of points $(\xi_L)_{l=1}^L$, $L \in \mathbb{N}$, on the sphere, which, when viewed in the ϑ-φ-plane, exhibits the structure of a rectangular grid consisting of rows and columns aligned to the two principal axes ϑ and φ. In the general case, we allow rows and columns to have different distances as illustrated in Figure 5.1. In the most common case in practical settings, the rows and columns are distributed uniformly in a certain domain $I \subseteq [0,\pi] \times [0,2\pi)$. We call a grid *regular*, if the distance between adjacent columns is constant. Furthermore we call it *complete* if its columns are even distributed uniformly on the torus $2\pi\,\mathbb{T}^1 := 2\pi(\mathbb{R}/\mathbb{Z})$ identified with the interval $[0,2\pi)$. We number the nodes row by row in increasing order where ϑ determines the row while φ determines the column. Furthermore, we let m be the number of rows and n the number of columns in a grid and we have therefore $\mathbf{\Psi} \in \mathbb{R}^{mn\times mn}$.

We now discuss three different setups of nodes and basis functions and derive the properties of $\mathbf{\Psi}$ they imply.

- **All basis functions are identical up to rotation.**
  This is the classical case for which the non-singularity of the resulting interpolation matrix $\mathbf{\Psi}$ is assured. The nodes might be distributed arbitrarily. Using the definition of the matrix $\mathbf{\Psi}$ from (2.1) it follows
  $$\psi_i\left(\xi_j\right) = G\left(\xi_i \cdot \xi_j\right) = \psi_j\left(\xi_i\right) \quad (1 \leq i,j \leq L).$$
  Hence, $\mathbf{\Psi}$ is symmetric and allows one to roughly halve the memory space needed to store the matrix.
- **The grid is regular and the basis function is the same for points in the same row.**
  This restriction allows for a decomposition of $\mathbf{\Psi}$ into quadratic blocks. A sub-matrix $\mathbf{\Psi}^{(k,l)}$ of $\mathbf{\Psi}$, defined by
  $$\mathbf{\Psi}^{(k,l)} := \left(\psi_{i,j}^{(k,l)}\right)_{i,j=1}^{n} \in \mathbb{R}^{n\times n} \quad (1 \leq k,l \leq m)$$

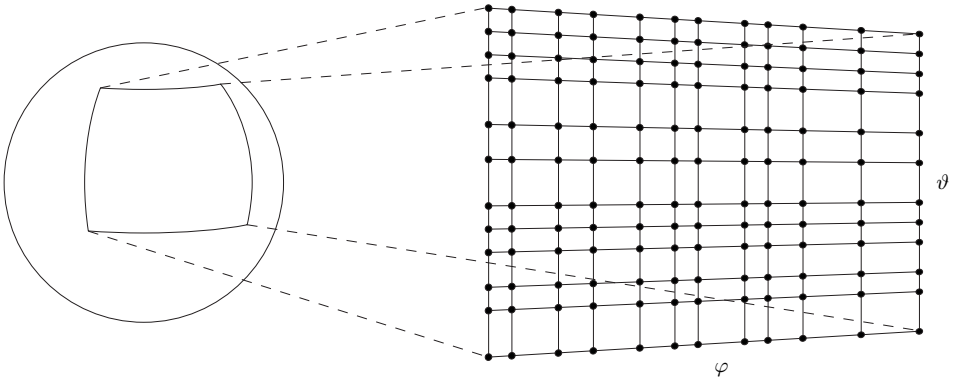

FIGURE 5.1. Mapping of a two-dimensional grid to a sphere. Every dot represents a node of the grid. Note that the distance between adjacent rows and columns varies and that the radius of the arcs, representing the rows of the grid, depends on the longitudinal angle ϑ, while the arcs corresponding to grid-columns all have equal radius. This is a direct consequence of the spherical coordinate system, we use.

and

$$\psi_{i,j}^{(k,l)} := \psi\left(\xi_{(k-1)n+i} \cdot \xi_{(l-1)n+j}\right)$$

contains all values that depend only on the inner products between all points in rows k and l. Therefore, the matrix $\boldsymbol{\Psi}$ has the representation

$$\boldsymbol{\Psi} = \begin{pmatrix} \boldsymbol{\Psi}^{(1,1)} & \boldsymbol{\Psi}^{(1,2)} & \dots & \boldsymbol{\Psi}^{(1,m)} \\ \boldsymbol{\Psi}^{(2,1)} & \boldsymbol{\Psi}^{(2,2)} & \dots & \boldsymbol{\Psi}^{(2,m)} \\ \vdots & \vdots & \ddots & \vdots \\ \boldsymbol{\Psi}^{(m,1)} & \boldsymbol{\Psi}^{(m,2)} & \dots & \boldsymbol{\Psi}^{(m,m)} \end{pmatrix} \in \mathbb{R}^{mn \times mn}.$$

Note that generally the matrix $\boldsymbol{\Psi}$ is no longer symmetric. But as a consequence of the data layout, the blocks $\boldsymbol{\Psi}^{(k,l)}$ have a very simple structure. Let ϑ_k, ϑ_l be the angles corresponding to rows k, l and φ_i, φ_j be the angles corresponding to columns i, j. Furthermore, we let $\delta > 0$ be the fixed latitudinal angle separating adjacent points in the same row. With G_k as the basis function used for row k, we get for a component

$$\psi_{(i,j)}^{(k,l)} = G_k\left((\vartheta_k, \varphi_i)^{\mathrm{T}} \cdot (\vartheta_l, \varphi_j)^{\mathrm{T}}\right)$$

of a block $\boldsymbol{\Psi}^{(k,l)}$ and analogously $\psi_{i-1,j-1}^{(k,l)}$ with $i, j > 1$, the identity

$$\begin{aligned} \psi_{i-1,j-1}^{(k,l)} &= G_k\left((\vartheta_k, \varphi_i - \delta)^{\mathrm{T}} \cdot (\vartheta_l, \varphi_j - \delta)^{\mathrm{T}}\right) \\ &= G_k\left(\cos\vartheta_k \cos\vartheta_l + \sin\vartheta_k \sin\vartheta_l \cos\left(\varphi_i - \delta - (\varphi_j - \delta)\right)\right) \\ &= G_k\left(\cos\vartheta_k \cos\vartheta_l + \sin\vartheta_k \sin\vartheta_l \cos\left(\varphi_i - \varphi_j\right)\right) \\ &= G_k\left((\vartheta_k, \varphi_i)^{\mathrm{T}} \cdot (\vartheta_l, \varphi_j)^{\mathrm{T}}\right) \\ &= \psi_{i,j}^{(k,l)}. \end{aligned}$$

Therefore, every block $\mathbf{\Psi}^{(k,l)}$ has the form of a *Toeplitz matrix*

$$\mathbf{\Psi}^{(k,l)} = \begin{pmatrix} \psi_{1,1}^{(k,l)} & \psi_{1,2}^{(k,l)} & \cdots & \psi_{1,n-1}^{(k,l)} & \psi_{1,n}^{(k,l)} \\ \psi_{2,1}^{(k,l)} & \psi_{1,1}^{(k,l)} & \cdots & \psi_{1,n-2}^{(k,l)} & \psi_{1,n-1}^{(k,l)} \\ \vdots & \vdots & \ddots & \vdots & \vdots \\ \psi_{n-1,1}^{(k,l)} & \psi_{n-2,1}^{(k,l)} & \cdots & \psi_{1,1}^{(k,l)} & \psi_{1,2}^{(k,l)} \\ \psi_{n,1}^{(k,l)} & \psi_{n-1,1}^{(k,l)} & \cdots & \psi_{2,1}^{(k,l)} & \psi_{1,1}^{(k,l)} \end{pmatrix}.$$

The first row and column completely determines all it's entries. Every Toeplitz matrix can be embedded into a circulant matrix of almost twice the size for every dimension. Since circulant matrices can be diagonalised by means of a multiplication with two Fourier matrices, this allows for the computation of a matrix-vector product with $\mathcal{O}(n \log n)$ arithmetic operations. Similarly, the solution of a linear system of equations, whose matrix is circulant, can also be calculated with $\mathcal{O}(n \log n)$ operations.

- **The grid is complete and the basis function is the same for points in the same row.**

  This case is very similar to the last one, except that further symmetries appear. We now require that also the angle that separates the first and the last point in each row equals δ. First, owing to the fact that the grid is now invariant to rotations along the axis through North and South pole by angles which are multiples of δ, each row of a block $\mathbf{\Psi}^{(k,l)}$ is a circularly shifted version of its successor:

$$\mathbf{\Psi}^{(k,l)} = \begin{pmatrix} \psi_{1,1}^{(k,l)} & \psi_{1,2}^{(k,l)} & \cdots & \psi_{1,n-1}^{(k,l)} & \psi_{1,n}^{(k,l)} \\ \psi_{1,n}^{(k,l)} & \psi_{1,1}^{(k,l)} & \cdots & \psi_{1,n-2}^{(k,l)} & \psi_{1,n-1}^{(k,l)} \\ \vdots & \vdots & \ddots & \vdots & \vdots \\ \psi_{1;3}^{(k,l)} & \psi_{1,4}^{(k,l)} & \cdots & \psi_{1,1}^{(k,l)} & \psi_{1,2}^{(k,l)} \\ \psi_{1;2}^{(k,l)} & \psi_{1,3}^{(k,l)} & \cdots & \psi_{1,n}^{(k,l)} & \psi_{1,1}^{(k,l)} \end{pmatrix}.$$

  Circulant matrices are completely determined by their first row or column. Second, another symmetry can be exploited. Since for every point the grid is also symmetric to the plane that contains the point and the two poles, the first row of a matrix-block $\mathbf{\Psi}^{(k,l)}$ is also symmetric to its centre.

We have described three cases, where symmetry properties can be used to reduce the storage space needed for $\mathbf{\Psi}$. Especially the third case is interesting, since there exist algorithms to treat the occurring types of matrices efficiently. How these algorithms work, is presented in the following section.

5.1. **Circulant Matrices and the Discrete Fourier Transform.** Circulant matrices can be multiplied with vectors efficiently. Let $\mathbf{A} := (a_{i,j}) \in \mathbb{R}^{n \times n}$ be a circulant matrix and $\mathbf{x} := (x_1, x_2, \ldots, x_n)^{\mathrm{T}} \in \mathbb{R}^n$ be a column-vector of length $n \in \mathbb{N}$. We have

$$(\mathbf{A}\mathbf{x})_i = \sum_{j=1}^{n} a_{i,j}\, x_j \quad (1 \le i \le n).$$

The circulant structure of $\mathbf{A}$ now gives $a_{i,j} = a_{(i-j \mod n)+1,1}$ which leads to

$$(\mathbf{A}\mathbf{x})_i = \sum_{j=1}^{n} a_{(i-j \mod n)+1,1}\, x_j.$$

If we now define the n-periodic sequences $\tilde{a} := (\tilde{a}_i)_{i \in \mathbb{Z}}$, $\tilde{x} := (\tilde{x}_i)_{i \in \mathbb{Z}}$, containing the elements of the first column of $\mathbf{A}$ and the elements of the vector $\mathbf{x}$, respectively,

by

$$\tilde{a}_i := a_{(i \mod n)+1,1},\ \tilde{x}_i := x_{(i \mod n)+1},$$

we can write the result of their discrete periodic convolution $\tilde{a} * \tilde{x}$ as

$$\begin{aligned}(\tilde{a} * \tilde{x})_i &= \sum_{j=0}^{n-1} \tilde{a}_{i-j}\, \tilde{x}_j = \sum_{j=0}^{n-1} a_{(i-j \mod n)+1,1}\, x_{(j \mod n)+1} = \sum_{j=0}^{n-1} a_{(i-j \mod n)+1,1}\, x_{j+1} \\ &= \sum_{j=1}^{n-1} a_{(i+1-j \mod n)+1,1}\, x_j = (\mathbf{A}\mathbf{x})_{i+1} \quad (0 \le i \le n-1)\,.\end{aligned}$$

We can calculate the result of the matrix-vector product $\mathbf{A}\,\mathbf{x}$ by a discrete periodic convolution of the vectors $\mathbf{a}$ and $\mathbf{x}$, where $\mathbf{a}$ is the column-vector containing the first column of $\mathbf{A}$. The *Discrete Convolution Theorem* tells that a discrete periodic convolution corresponds to a component-wise multiplication in the frequency domain. If we now denote an application of the discrete Fourier transform (DFT) to a vector $\mathbf{x}$ by $\mathrm{DFT}\,(\mathbf{x})$ and analogously an application of the inverse transform (IDFT) by $\mathrm{IDFT}\,(\mathbf{x})$, we therefore get

$$\mathrm{DFT}\,(\mathbf{A}\,\mathbf{x}) = \mathrm{DFT}\,(\mathbf{a}) \odot \mathrm{DFT}\,(\mathbf{x}) \tag{5.1}$$

and

$$\mathbf{A}\,\mathbf{x} = \mathrm{IDFT}\,(\mathrm{DFT}\,(\mathbf{a}) \odot \mathrm{DFT}\,(\mathbf{x}))\,,$$

where $\odot$ means the component-wise multiplication or *Hadamard product*. But there is more we can learn from (5.1): If we rewrite the application of a DFT as a multiplication with a Fourier matrix $\mathbf{F_n}$, then the component-wise multiplication of $\mathrm{DFT}\,(\mathbf{a}) = \mathbf{F}_n\,\mathbf{a}$ and $\mathrm{DFT}\,(\mathbf{x}) = \mathbf{F}_n\,\mathbf{x}$ can be written as $\mathrm{diag}\,(\mathbf{F}_n\,\mathbf{a})\ \mathbf{F}_n\,\mathbf{x}$. This yields

$$\mathbf{F}_n\,\mathbf{A}\,\mathbf{x} = \mathrm{diag}\,(\mathbf{F}_n\,\mathbf{a})\ \mathbf{F}_n\,\mathbf{x}.$$

Since Fourier matrices are orthogonal, i.e. $\mathbf{I} = \mathbf{F}_n^{-1}\,\mathbf{F}_n = \mathbf{F}_n^{\mathrm{H}}\,\mathbf{F}_n$ with $\mathbf{I}$ being the identity matrix, we obtain

$$\mathbf{F}_n\,\mathbf{A}\,\mathbf{F}_n^{\mathrm{H}}\,\mathbf{F}_n\,\mathbf{x} = \mathrm{diag}\,(\mathbf{F}_n\,\mathbf{a})\ \mathbf{F}_n\,\mathbf{x}.$$

We conclude $\mathbf{F}_n\,\mathbf{A}\,\mathbf{F}_n^{\mathrm{H}} = \mathrm{diag}\,(\mathbf{F}_n\,\mathbf{a})$, i.e. the matrix $\mathbf{A}$ can be diagonalised by two Fourier matrices $\mathbf{F}_n$.

The component-wise multiplication of $\mathrm{DFT}\,(\mathbf{a})$ and $\mathrm{DFT}\,(\mathbf{x})$ can be computed with $\mathcal{O}\,(n)$ arithmetic operations. The computational complexity of the multiplication algorithm is therefore determined by the application of DFT and IDFT. These steps require $\mathcal{O}\,(n\,\log n)$ *floating point operations (flops)*, if a fast Fourier transform algorithm (FFT) is used.

We now turn to systems of linear equations $\mathbf{A}\,\mathbf{x} = \mathbf{b}$ whose system matrix is circulant. We multiply with the Fourier matrix $\mathbf{F}_n$ from the left and by recalling $\mathbf{F}_n^{\mathrm{H}}\,\mathbf{F}_n = \mathbf{I}$ we get

$$\mathbf{F}_n\,\mathbf{A}\,\mathbf{F}_n^{\mathrm{H}}\,\mathbf{F}_n\,\mathbf{x} = \mathbf{F}_n\,\mathbf{b}.$$

Using that $\mathbf{F}_n\ \mathbf{A}\ \mathbf{F}_n^{\mathrm{H}}$ is a diagonal matrix whose main diagonal entries can be computed with $\mathcal{O}\,(n \log n)$ flops using an FFT, the system has been transformed into a very simple form and we can solve it with $\mathcal{O}\,(n)$ arithmetic operations and obtain the vector $\mathbf{F}_n\,\mathbf{x}$. A final application of the inverse FFT gives the sought solution $\mathbf{x}$. In total, we need $\mathcal{O}\,(n \log n)$ flops.

Block matrices $\mathbf{\Psi}$ with circulant blocks can be handled by a reduction to the algorithm for circulant matrices. For example, we write the system $\mathbf{\Psi}\,\mathbf{x} = \mathbf{b}$ as

$$\begin{pmatrix} \mathbf{\Psi}^{(1,1)} & \mathbf{\Psi}^{(1,2)} & \dots & \mathbf{\Psi}^{(1,m)} \\ \mathbf{\Psi}^{(2,1)} & \mathbf{\Psi}^{(2,2)} & \dots & \mathbf{\Psi}^{(2,m)} \\ \vdots & \vdots & \ddots & \vdots \\ \mathbf{\Psi}^{(m,1)} & \mathbf{\Psi}^{(m,2)} & \dots & \mathbf{\Psi}^{(m,m)} \end{pmatrix} \begin{pmatrix} \mathbf{x}^{(1)} \\ \mathbf{x}^{(2)} \\ \vdots \\ \mathbf{x}^{(m)} \end{pmatrix} = \begin{pmatrix} \mathbf{b}^{(1)} \\ \mathbf{b}^{(2)} \\ \vdots \\ \mathbf{b}^{(m)} \end{pmatrix},$$

with circulant blocks $\mathbf{\Psi}^{(i,j)}$, where $\mathbf{\Psi}^{(i,j)} \in \mathbb{R}^{n\times n},\ \mathbf{x}^{(i)}, \mathbf{b}^{(i)} \in \mathbb{R}^n$. Using the results for circulant matrices and defining

$$\mathbf{F}_{m,n} := \mathbf{I}_m \otimes \mathbf{F}_n,$$

with the usual *Kronecker product* $\otimes$, one can write

$$\mathbf{F}_{m,n}\ \mathbf{\Psi}\ \mathbf{F}_{m,n}^{\mathrm{H}}\ \mathbf{F}_{m,n}\ \mathbf{x} = \mathbf{F}_{m,n}\ \mathbf{b}$$

where $\mathbf{F}_{m,n}\ \mathbf{\Psi}\ \mathbf{F}_{m,n}^{\mathrm{H}}$ is a matrix consisting of m^2 diagonal blocks. By reordering rows and columns properly, which would correspond to further multiplications with permutation matrices, we obtain a system of linear equations with a block-diagonal matrix. Each of the m blocks of dimension $n \times n$ represents an independent system of linear equations.

For an asymptotic complexity analysis, we now require m to be of comparable size as n, hence $m = cn$ for some $c \in \mathbb{R}$. In the algorithm, one must first calculate $m^2 + m$ discrete Fourier transforms. Each of these transforms has length n and therefore requires $\mathcal{O}(n \log n)$ flops. In total, this step accumulates to $\mathcal{O}\left(m^2 n \log n\right)$ flops. Next, we must calculate m matrix-vector products, or must solve m linear systems of equations, in each case of dimension $n \times n$. Depending on the concrete algorithms used for these steps, we can count the complexity for each of them by $C(n)$. We only know that one can't get better than $C(n) = \mathcal{O}\left(n^2\right)$ and that $C(n) = \mathcal{O}\left(n^3\right)$ is always possible. Together, this gives a complexity of $\mathcal{O}(mC(n))$ for this step. The last step, the computation of IDFTs for each of the m vector-blocks of the intermediate result, needs $\mathcal{O}(mn \log n)$ flops. So the described method requires in total

$$\mathcal{O}\left(m^2 n \log n + mC(n) + mn \log n\right) = \mathcal{O}\left(m^3 \log n + mC(m)\right)$$

flops. In general, methods not exploiting the matrix structure have a complexity of $\mathcal{O}(C(nm))$ flops which is at least $\mathcal{O}\left(m^4\right)$ flops. Algorithm 1 summarises the described method for systems of linear equations whose system matrix consists of circulant blocks.

6. An Application

In this final section, we present an application of the previously described approximation schemes to real-life data.

For texture analysis in crystallography, spherical data on a regular grid are processed and reviewed. However, these measurements today are still very time consuming, therefore limiting the affordable resolution of the result.

On this basis, representations with Poisson kernels were calculated for a given data set. These representations can be viewed as a stochastic model. Since we solve an interpolation problem, the resulting function as a linear combination of rotated kernel functions coincides with the measured data on the grid, regardless of the parametrisation of the kernels. But from a numerical point of view, a good adjustment of the parameters is the key. If a small value h is used for all basis functions, the interpolation matrix $\mathbf{\Psi}$ becomes nearly singular, since the kernels are close to constant functions. On the other hand, the use of a value close to

Algorithm 1 Solving systems of linear equations with block-matrix with circulant blocks

Input: $n, m \in \mathbb{N}$, for $j, k = 1, \dots, m$ the block-matrix $\mathbf{\Psi} \in \mathbb{R}^{nm \times nm}$ with circulant blocks, represented by vectors $\mathbf{a}^{(j,k)} \in \mathbb{R}^n$ containing the first column of each block, the right-hand side $\mathbf{b} \in \mathbb{R}^{nm}$ given by sub-vectors $\mathbf{b}^{(j)} \in \mathbb{R}^n$ for $j = 1, \dots, m$.

for $j = 1, \dots, m$ **do**
  Compute $\hat{\mathbf{b}}^{(j)} := \mathrm{DFT}\left(\mathbf{b}_j\right)$ by an FFT of length n.
  for $k = 1, \dots, m$ **do**
    Compute $\hat{\mathbf{a}}^{(j,k)} := \mathrm{DFT}\left(\mathbf{a}^{(j,k)}\right)$ by an FFT of length n.
  end for
end for

for $j = 1, \dots, m$ **do**
  Compute $\hat{\mathbf{x}}^{(j)}$ as the solution of the m-th system of linear equations.
  Compute $\mathbf{x}^{(j)} := \mathrm{IDFT}\left(\hat{\mathbf{x}}^{(j)}\right)$ by an inverse FFT.
end for

Output: $\mathbf{x} \in \mathbb{R}^{nm}$ as solution of the system $\mathbf{\Psi}\,\mathbf{x} = \mathbf{b}$.
Asymptotic complexity: $\mathcal{O}\left(m^2 n \log n + mC\left(n\right) + mn \log n\right)$ flops.

1 pushes $\mathbf{\Psi}$ towards the unity matrix, making the calculation more stable, but the model represented might not be very reasonable. Therefore, the calculated representation was evaluated at a refined resolution.

At first, only rotated versions of a single kernel with a fixed h were used. Results for different values of h are shown in Figures 6.1 and 6.2. One observes that, depending on h, the quality of the result strongly differs comparing the equatorial and the polar regions. Clearly, due to the topology of the sphere, a single basis function near the poles has a noticeably higher impact on it's neighbour points than one located near the equator, a fact that causes numerical instabilities. On the other hand, increasing h makes the effective support of the basis functions in the equatorial region very small.

This leads to the idea of using kernels with different spatial densities. According to [9, p. 933], a properly normalised Poisson kernel $Q_h\left(\eta \cdot \xi\right)$ as a function of $\xi \in \mathbb{S}^2$ for fixed $\eta \in \mathbb{S}^2$ can be regarded as a probability density function and the variance σ is given by

$$\sigma^2 = \left(\frac{1 - h^2}{1 + h^2}\right).$$

This formula can be used to derive an automatic procedure that adjusts the parameter h for each row of a spherical grid, thereby controlling the overlap of the spherical basis functions $G_l\left(\xi\right) = Q_{h_l}\left(\xi_l \cdot \xi\right)$ for $l = 1, \dots, L$. Figure 6.3 shows the result after application of this procedure.

This closes our investigation. For further improvements, the representation of sharp peaks in the input data must be taken into account. But therefore, one must leave the regular structure of the interpolation matrix $\mathbf{\Psi}$. Here, it might be useful, to compute a coarse approximation on a regular grid with the proposed method and incorporate sharp peaks afterwards. For example, one could solve the interpolation problem by using an iterative method for systems of linear equations. The solution calculated first could here be used as the initial solution, in order to reduce the number of iterations needed.

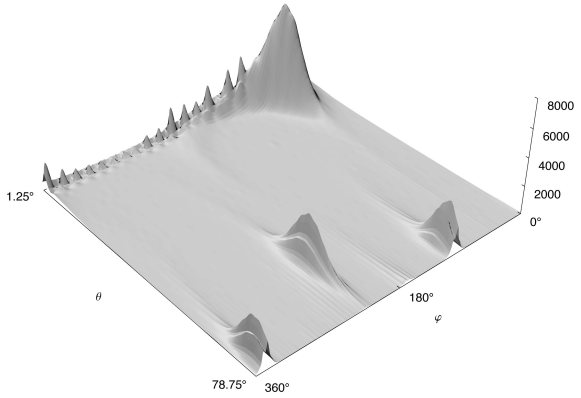

FIGURE 6.1. The interpolated data evaluated on a grid with four-fold resolution. The kernels were parametrised with $h = 0.96$. The result shows ripple artifacts near the North pole and also negative values – in this case not admissible from the application.

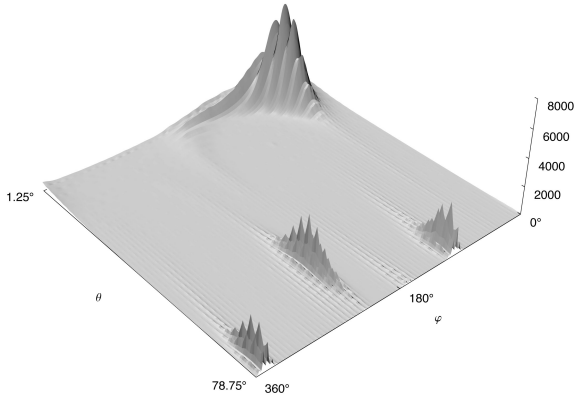

FIGURE 6.2. The same data as in Figure 6.1 but now for $h = 0.98$. Artifacts near the pole are reduced but the spatial density of the spherical basis functions is to low to provide a reasonable approximation far from the pole.

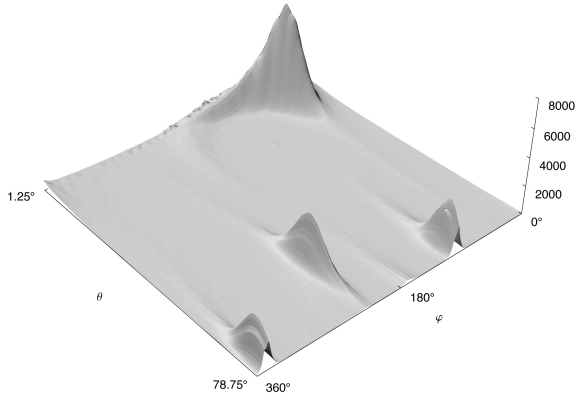

FIGURE 6.3. The same data as in Figure 6.1 now using automatic spatial density adjustment for the spherical basis functions. Some artifacts remain near the pole but the overall approximation result is smooth.

References

[1] Åke Björk, *Numerical Methods for Least Squares Problems*, SIAM, Philadelphia, 1996.

[2] K. G. v.d. Boogaart, R. Hielscher, J. Prestin, and H. Schaeben, *Application of the radial basis function method to texture analysis*, J. Comput. Appl. Math. (to appear).

[3] M.D. Buhmann, *Radial Basis Functions*, Cambridge University Press, Cambridge, 2003.

[4] D. Chen, V. A. Menegatto, and X. Sun, *A necessary and sufficient condition for strictly positive definite functions on spheres*, Proc. Am. Math. Soc. **131** (2003), 2733–2740.

[5] W. Freeden, T. Gervens, and M. Schreiner, *Constructive Approximation on the Sphere*, Oxford University Press, Oxford, 1998.

[6] Q. T. Le Gia, *Galerkin approximation for elliptic PDEs on spheres*, J. Approx. Theory **130** (2004), 125–149.

[7] F. J. Narcowich and J.D. Ward, *Scattered data interpolation on spheres: error estimates and locally supported basis functions*, SIAM J. Math. Anal. **33** (2002), 1393–1410.

[8] Kunis. S. and D. Potts, *Fast spherical Fourier algorithms*, J. Comput. Appl. Math. **161** (2003), 75–98.

[9] Ta-Hsin Li, *Multiscale Representation and Analysis of Spherical Data by Spherical Wavelets*, SIAM J. Sci. Comput. **21** (1999), 924–953.

[10] C. Müller, *Spherical Harmonics*, Lecture Notes in Mathematics, Vol. 17, Springer Verlag, Berlin, 1966.

[11] R. Opfer, *Multiscale Kernels*, Shaker Verlag, Aachen, 2005.

[12] I. J. Schoenberg, *Positive definite functions on spheres*, Duke Math. J. **9** (1942), 98–108.

[13] Gábor Szegő, *Orthogonal Polynomials*, Amer. Math. Soc. Colloq. Publ., Amer. Math. Soc., Providence, 1975.

J. Keiner & J. Prestin
Institute of Mathematics
University of Lübeck
Wallstraße 40, 23560, Lübeck, Germany
{keiner, prestin}@math.uni-luebeck.de
www.math.uni-luebeck.de/{keiner, prestin}